Solvent thermal synthesis and gas-sensing properties of Fe-doped ZnO

Wen-Hui Zhang · Wei-De Zhang · Jue-Fei Zhou

Abstract In this study, pure ZnO microbullets, ZnO–ZnFe$_2$O$_4$ composite, and ZnO–Fe$_2$O$_3$–ZnFe$_2$O$_4$ composite with micron structured balloons, rods, and particles were prepared by a simple solvent thermal process using methanol or ethanol as solvents. The influence of solvents on the composition and morphology of the products was studied, and their gas-sensing properties were also investigated. The morphology of ZnO microbullets synthesized in ethanol is similar to but more uniform than that of ZnO microbullets synthesized in methanol. The Fe-doped ZnO synthesized in ethanol contains many micron particles homogeneously dispersing on the surface of the microbullets, which is composed of hexagonal wurtzite ZnO and franklinite ZnFe$_2$O$_4$, while Fe-doped ZnO prepared in methanol consists of micron structured balloons, rods, and particles, which is composed of hexagonal wurtzite ZnO, hematite Fe$_2$O$_3$, and franklinite ZnFe$_2$O$_4$. Compared with pure ZnO and ZnO–ZnFe$_2$O$_4$ composite, the ZnO–Fe$_2$O$_3$–ZnFe$_2$O$_4$ composite presented high response, rapid response/recovery characteristics, good selectivity, and excellent stability to acetone at relatively low operating temperature of 190 °C. This sensor could detect acetone in wide range of 1–1000 ppm, which was expected to be a promising gas sensor for detecting acetone.

Introduction

Zinc oxide (ZnO) has attracted attention because of the wide range of applications such as solar cells, luminescent, electrical and acoustic devices, as well as chemical sensors [1–4]. ZnO has been extensively investigated as a gas sensing material for practical applications, such as gas leak detection and environmental monitoring. Generally, ZnO sensors provide a wide variety of advantages, such as low cost, short response time, easy manufacturing, and small in size, compared with the traditional analytical instruments. However, the traditional ZnO gas sensors suffer from several problems such as high operating temperature, poor selectivity, and relatively low response, which limit their applications in real-time gas sensing. Doping is an important and effective way to improve gas-sensing properties. Noble metals [5–7] or oxides such as SnO$_2$ [8], TiO$_2$ [9], CuO [10], CeO$_2$ [11], Fe$_2$O$_3$ [12], ZnFe$_2$O$_4$ [13, 14] were often used as dopants, but ZnO–Fe$_2$O$_3$–ZnFe$_2$O$_4$ composite has not been reported.

Acetone is a colorless and transparent liquid. It is volatile, highly flammable, and the most commonly used organic solvent and exists widely in the air of production place and laboratory. Once the body inadvertently inhales acetone, it will stimulate the respiratory tract and cause headache and dizziness. Therefore, real-time detection of acetone in the environment for human health and production safety is very important. However, most of ZnO-based gas sensors focus on ethanol [15], NO$_2$ [16], CO [17], O$_2$ [18], and H$_2$ [19], and rare studies concern the acetone sensing characteristics. Moreover, the cross-sensitivity between acetone and ethanol troubles many researchers since the sensing behaviors of the sensors to ethanol and acetone are similar in most investigations [20–27]. It is foreseen that fabrication of a selective gas sensor to effectively distinguish between acetone and ethanol is

W.-H. Zhang · W.-D. Zhang (✉) · J.-F. Zhou
Nano Science Research Center, School of Chemistry and Chemical Engineering, South China University of Technology, 381 Wushan Road, Guangzhou 510640, People's Republic of China
e-mail: zhangwd@scut.edu.cn

useful in future science. In this study, ZnO–Fe_2O_3–$ZnFe_2O_4$ composite have been successfully prepared by a facile one-step solvent thermal process, and the results of gas sensing test indicate that gas sensor based on ZnO–Fe_2O_3–$ZnFe_2O_4$ composite can selectively detect acetone at relatively low temperature of 190 °C.

Experimental section

ZnO and ZnO–Fe_2O_3–$ZnFe_2O_4$ composite were prepared by a solvent thermal process using commercial ZnO powder and $Fe(NO_3)_3 \cdot 3H_2O$ as precursors and they were all of analytical grade and were used without further purification. Firstly, 0.10 g ZnO powder was dispersed into 30 mL methanol without or with 0.010 M $Fe(NO_3)_3$. The pH value of the mixed solution was adjusted to 3 by 5 M HNO_3 under stirring and all the ZnO powder was dissolved. The solution was transferred into a 50.0 mL Teflon-lined stainless steel autoclave. Then, the autoclave was sealed tightly, rapidly heated to 240 °C, and maintained at 240 °C for 30 min. After the reaction, the autoclave was naturally cooled down to room temperature. The precipitate was filtered; then washed several times with distilled water, and dried at 60 °C. The obtained products were labeled as sample 1 (pure ZnO) and sample 2 (Fe-doped), respectively.

The effect of solvent on the composition and morphology of samples was also studied. Methanol was replaced by ethanol in the above procedure, and the obtained products were labeled as sample 3 (pure ZnO) and sample 4 (Fe-doped), respectively.

The crystal structure of the obtained samples was characterized by a Shimadzu XD-3A X-ray diffractormeter (XRD) with Cu Kα radiation ($\lambda = 0.15406$ nm). XRD patterns were recorded from 10 to 70° at a scanning step of 4° min^{-1}. The morphology of the samples was observed by a field-emission scanning electron microscope (SEM) (Philips XL 30 FEG). Surface elemental composition of the samples was analyzed by an energy-dispersive X-ray spectrometer (EDS). The Brunauer–Emmett–Teller (BET) surface area was determined by a ST-08A measuring instrument (Beijing Analysis Instruments Technical Company, Beijing, China).

Details of gas sensing measurement were operated as reported in Ref [28]. The powder samples were dry-ground and then wet-ground with an organic binder to form a paste. The resulting paste was coated on an Al_2O_3 tube with a pair of Au electrodes attached with Pt wires. After dried in air, it is sintered at 600 °C for 2 h. Finally, the electrodes were fixed on the circuit for measurement. The fabricated sensing element was firstly aged at 190 °C for 240 h. Gas samples were directly injected into a test jar and

mixed with the air inside. Liquid samples were injected on a heater in the jar for evaporation. The constant voltage of the measuring system was fixed at 3.5 V in our experiment. The response/recovery time of the sensor is defined as the time needed to reach 90% of the original resistance. The gas response (S) was defined as the ratio (R_a/R_g) of the resistance in air (R_a) and in a sample gas or vapor (R_g).

Results and discussion

The crystalline structure of samples 1 and 2 prepared by using methanol as solvent was characterized by using X-ray diffraction technology, as displayed in Fig. 1. It can be seen from Fig. 1a that all the well-crystallized diffraction peaks of sample 1 are well indexed to the standard hexagonal phase ZnO (JCPDS 36-1451), and the absence of impurity peaks suggests high purity of the prepared sample. The XRD patterns of sample 2 calcined at 300 (Fig. 1e), 450 (Fig. 1f) and 600°C (Fig. 1g) all contained diffraction peaks from hexagonal wurtzite ZnO (JCPDS 36-1451), hematite Fe_2O_3 (JCPDS 33-0664), and franklinite $ZnFe_2O_4$ (JCPDS 22-1012). Those characteristic peaks of Fe_2O_3 and $ZnFe_2O_4$ were obviously weaker than those of ZnO. The intensity of the peaks increased upon the increase of calcining temperature. According to the Scherrer equation, the grain size of ZnO calcined at 300, 450, and 600°C was calculated to be 20, 21, and 36 nm, respectively, while that of the Fe_2O_3 was 21, 24, and
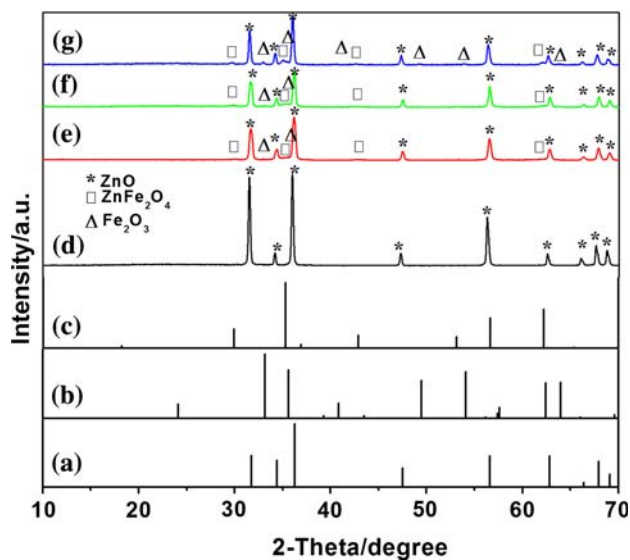

Fig. 1 XRD patterns of samples prepared using methanol as solvent, (*a*) standard pattern of ZnO (JCPDS 36-1451), (*b*) standard pattern of Fe_2O_3 (JCPDS 33-0664), (*c*) standard pattern of $ZnFe_2O_4$ (JCPDS 22-1012), (*d*) samples 1 and 2 calcined at (*e*) 300 °C, (*f*) 450 °C, and (*g*) 600 °C

42 nm, and that of the $ZnFe_2O_4$ was 10, 11, and 12 nm, respectively. All the grain size of the crystals increased with the increase of calcining temperature. It can be concluded that ZnO–Fe_2O_3–$ZnFe_2O_4$ composite was successfully synthesized in the solution with methanol as a solvent.

The SEM images of pure ZnO and ZnO–Fe_2O_3–$ZnFe_2O_4$ composite are shown in Fig. 2. It can be seen from Fig. 2a, b that the morphology of sample 1 was microbullets, some of which were broken in the middle. Figure 2b illustrates the amplificatory ZnO microbullets with some nanopores on the surface. The length and medial width of ZnO microbullets were 10–20 μm and 3.5–5.4 μm, respectively. The morphology of sample 2 contained microballoons, micron rods, and micron particles (Fig. 2c, d). The length and the medial width of microballoons were 10–20 μm and 3.5–5.4 μm, respectively; the length and the diameter of the micron rods were about 6.5 μm and 900 nm, respectively; the average diameter of particles was 925 nm. Many nano pores on the surface of different morphologies especially microballoons were observed (Fig. 2d). The specific surface area of the ZnO–Fe_2O_3–$ZnFe_2O_4$ composite was about 48.1 $m^2\,g^{-1}$, indicating that the ZnO–Fe_2O_3–$ZnFe_2O_4$ composite presented a larger surface area than that of pure ZnO (2.1 $m^2\,g^{-1}$). The EDS results of the ZnO–Fe_2O_3–$ZnFe_2O_4$ composite revealed (Table 1) that the microballoons were only composed of O and Zn, and the quantitative analysis results indicated that the molar ratio of O and Zn was approximately 1:1.51, suggesting that the microballoons were composed of ZnO. However, both the rods and the

Table 1 Composition of sample 2 based on EDS analysis

Morphology	O (atom%)	Zn (atom%)	Fe (atom%)
Micron balloons	39.8	60.2	–
Micron rods	43.4	49.2	7.53
Micron particles	52.3	17.0	30.7

particles were composed of O, Zn, and Fe, and the molar ratio of O, Zn, and Fe was approximately 1:1.1:0.173 and 1:0.324:0.587, respectively, indicating that both the micron rods and micron particles were doped with Fe, and the micron particles contained more Fe.

To develop a better understanding of the synthesis of the products, the influence of solvents was investigated in this study. Figure 3 shows the XRD patterns of samples 3 and 4 prepared using ethanol as a solvent. All the diffraction peaks of sample 3 could be perfectly indexed as the hexagonal wurtzite structure ZnO (JCPDS 36-1451), while all the reflection peaks of sample 4 calcined at 600 °C could be readily indexed to hexagonal wurtzite ZnO (JCPDS 36-1451) and franklinite $ZnFe_2O_4$ (JCPDS 22-1012). The fact that no distinct peaks corresponding to Fe_2O_3 was formed at the calcining temperature of 600 °C indicated that ZnO–$ZnFe_2O_4$ composite were synthesized in ethanol.

The SEM images of sample 3 (pure ZnO) and sample 4 (Fe-doped) are shown in Fig. 4a, b, respectively. The morphology of pure ZnO was microbullets, similar to but more uniform than that of sample 1. Furthermore, only a few microbullets were broken in the middle. The length and the

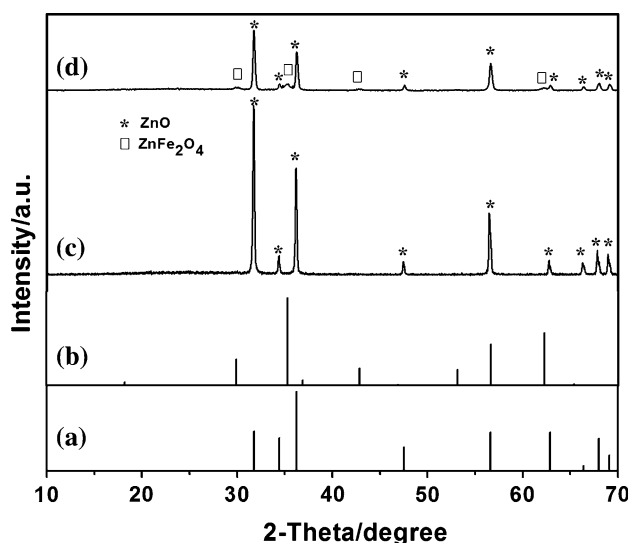**Fig. 2** SEM images of **a**, **b** sample 1 and **c**, **d** sample 2
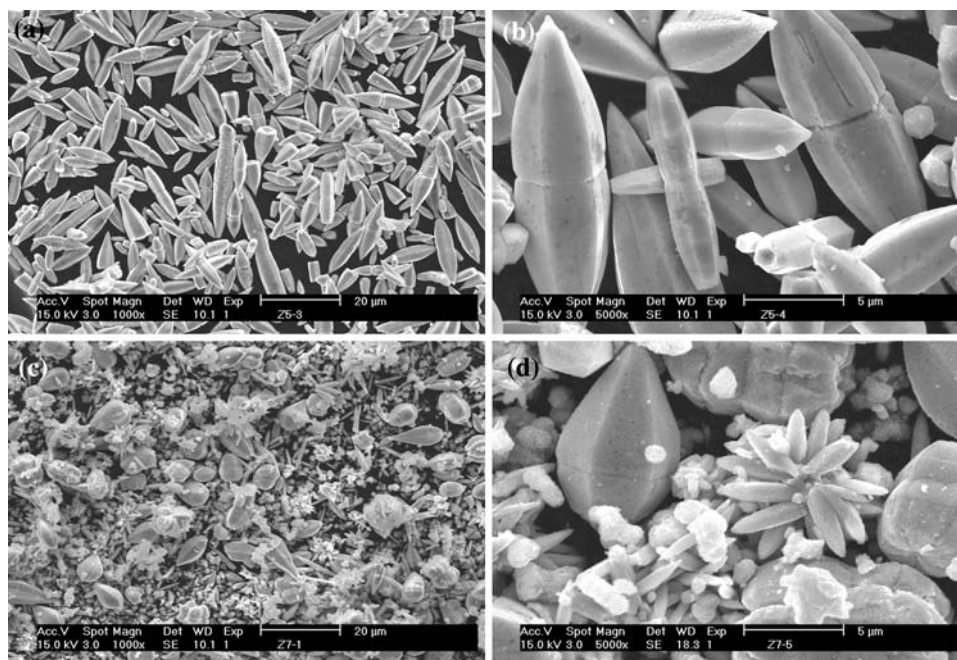
Fig. 3 XRD patterns of (*a*) standard pattern of ZnO (JCPDS 36-1451), (*b*) standard pattern of ZnFe$_2$O$_4$ (JCPDS 22-1012), (*c*) sample 3, and (*d*) sample 4 prepared using ethanol as solvent
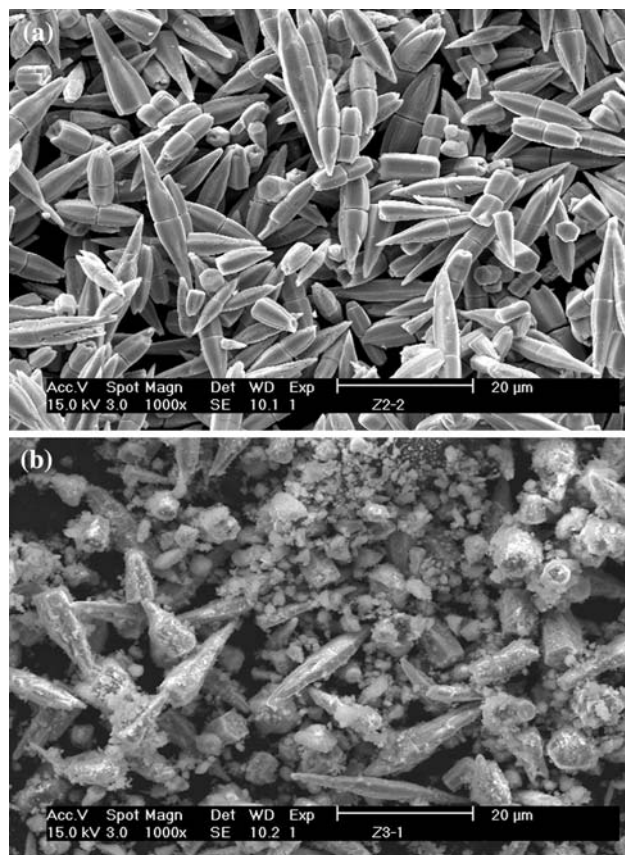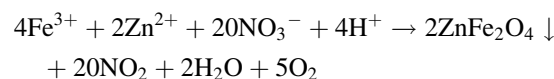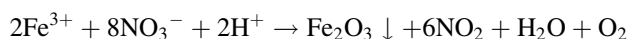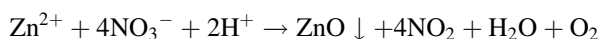

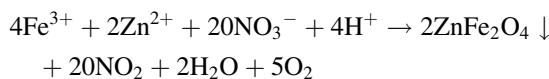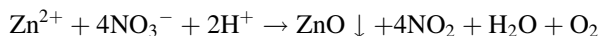**Fig. 4** SEM images of **a** sample 3 and **b** sample 4

medial width of ZnO microbullets were 10–20 μm and 2.5–3.5 μm, respectively. The morphology of ZnO–ZnFe$_2$O$_4$ composite was microbullets, with many micron particles homogeneously on their surface. The specific surface area of

the ZnO–ZnFe$_2$O$_4$ composite was 18.2 m^2 g^{-1}, which was larger than that of pure ZnO (1.0 m^2 g^{-1}). It is obvious that solvents affect the morphology of the products.

Although the mechanism leading to the formation of oxides will need further investigation, a possible reaction mechanism can be proposed on the basis of our experimental results. In the precursor solution, the Zn source was primarily in the form of Zn^{2+} and NO$_3^-$. In fact, iron nitrate dissolved in an aqueous solution and ionized to Fe^{3+} and NO$_3^-$, and the direct high temperature decomposition of nitrate ($4Fe^{3+} + 12NO_3^- \rightarrow 2Fe_2O_3\downarrow + 12NO_2 + 3O_2$) could take place [29]. While in the acidic methanol thermal solution with high temperature and high pressure, Zn^{2+}, H$^+$, and iron nitrate should react, and the reaction scheme can be presented as follows:

$$Zn^{2+} + 4NO_3^- + 2H^+ \rightarrow ZnO \downarrow + 4NO_2 + H_2O + O_2$$

$$2Fe^{3+} + 8NO_3^- + 2H^+ \rightarrow Fe_2O_3 \downarrow + 6NO_2 + H_2O + O_2$$

$$4Fe^{3+} + 2Zn^{2+} + 20NO_3^- + 4H^+ \rightarrow 2ZnFe_2O_4 \downarrow$$
$$+ 20NO_2 + 2H_2O + 5O_2$$

While in the acidic ethanol thermal solution and at high temperature and high pressure, the reactions can be proposed as follows:

$$Zn^{2+} + 4NO_3^- + 2H^+ \rightarrow ZnO \downarrow + 4NO_2 + H_2O + O_2$$

$$4Fe^{3+} + 2Zn^{2+} + 20NO_3^- + 4H^+ \rightarrow 2ZnFe_2O_4 \downarrow$$
$$+ 20NO_2 + 2H_2O + 5O_2$$

The solvent is the important factor for controlling the nucleation. Methanol or ethanol, in fact, provides an appropriate medium for the hydrolysis of nitrate that yield ZnO through the condensation route. Methanol or ethanol also acted as a good dispersing agent during the reaction. The polarity and saturated vapor pressure of solvents were found to exert influence on the products under thermal conditions. So, ZnO–Fe$_2$O$_3$–ZnFe$_2$O$_4$ composite with microballoons, rods, and particles was synthesized with methanol as a solvent.

In order to determine the optimum operating temperature of the sensors, response of sensors to 50 ppm acetone at different operating temperature was examined, as illustrated in Fig. 5. Upon increase of the operating temperature, the response of sensors based on samples 1, 3, and 4 to 50 ppm acetone all increased from 150 to 330 °C and reached the maximum of 15, 7, and 8 at 330 °C, respectively. However, the response of the sensor based on sample 2 increased from 150 to 240 °C and reached the maximum at 240 °C. Compared with other sensors, the response of sample 2 sensor to 50 ppm acetone was the highest at low temperature (≤240° C). The gas-sensing properties of sample 2 sensor were further investigated in details.
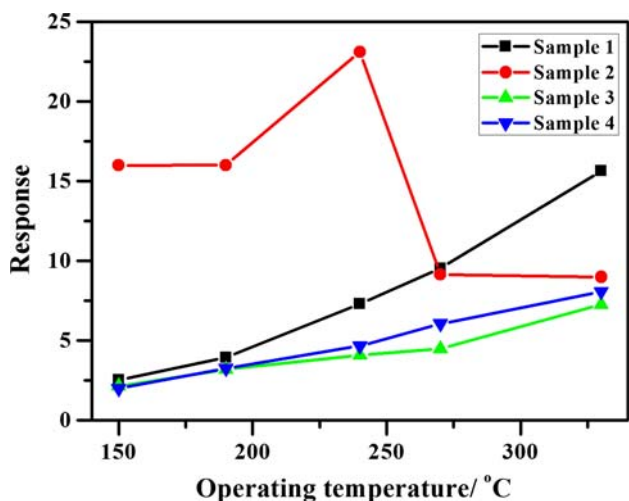
Fig. 5 Response of sensors to 50 ppm acetone at different operating temperatures

Table 2 Response/recovery time of sample 2 sensor at different operating temperatures

Operating temperature (°C)	150	190	240	270	330
Response time/s	17	5	5	5	5
Recovery time/s	65	29	13	3	2

Response and recovery time are important parameters of gas sensors. The response/recovery time of sample 2 sensor to 50 ppm acetone at different operating temperatures are summarized in Table 2. The response time at 150 °C was about 17 s, but it reduced to 5 s at 190–270 °C. The recovery time also decreased with increase of the operating temperature, from 65 s at 150 °C to 2 s at 330 °C. The increase of the operating temperature can accelerate desorption and catalytic conversion of the target molecules, thus shortening the recovery time. The results revealed this sensor with rapid response/recovery characteristics at operating temperature of 190–270 °C. To meet the need of both fast response/recovery requirement and low energy consumption, the operating temperature was controlled at 190 °C in our experiments.

At 190 °C, the typical response/recovery curve of the sensor based on sample 2 to various concentrations of acetone (1–1000 ppm) is shown in Fig. 6a. When acetone was introduced, the response of the sensor appeared immediately. In addition, its reversibility and repeatability were also very good. In consecutive tests of the sensor to acetone with various concentrations, the response and recovery are still very good to low concentration of acetone even after exposure to as high concentration of acetone as 1000 ppm. Figure 6b illustrates the response of sample 2 sensor to various concentrations of acetone at 190 °C. The sensor exhibits excellent response in the range of
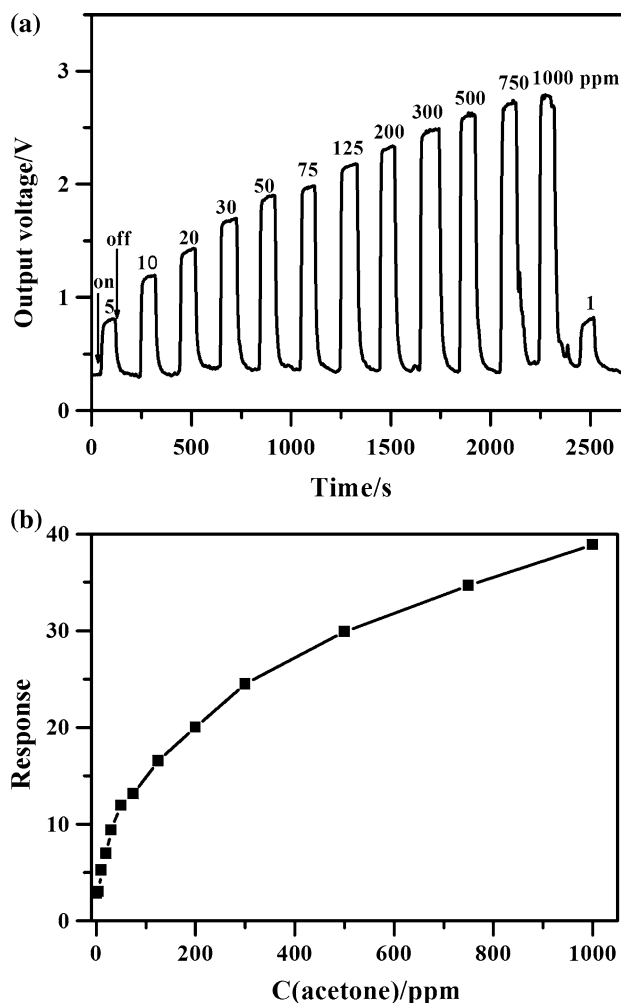

Fig. 6 a Response/recovery curve and b response of sample 2 sensor to various concentrations of acetone at 190 °C

1–1000 ppm with the minimum of 1 ppm ($S = 2.8$). The response to acetone increased with the increase of the concentration, suggesting that it could meet the application demand. The fast response/recovery characteristics remained when detecting as high concentration of acetone as 1000 ppm. The response and recovery time were less than 10 and 60 s, respectively. Thus, it can be concluded that the sensor could detect acetone in the range of 1–1000 ppm with prompt response and recovery.

The sensing properties of the sensor based on sample 2 to other gases or vapors such as CO, H_2, CH_4, NH_3, LPG, NO_2, benzene, toluene, ethanol, methanol, acetone, and formaldehyde were also examined. The response to the above gases or vapors of 50 ppm at 190 °C is shown in Fig. 7. One can see that this sensor showed the highest response to acetone (16), while its response to methanol, ethanol, toluene, and formaldehyde is 7, 8, 5.8, and 5.5, respectively. The response of the sensor to other gases or vapors such as CO, H_2, NO_2, methane, LPG, water, etc., is
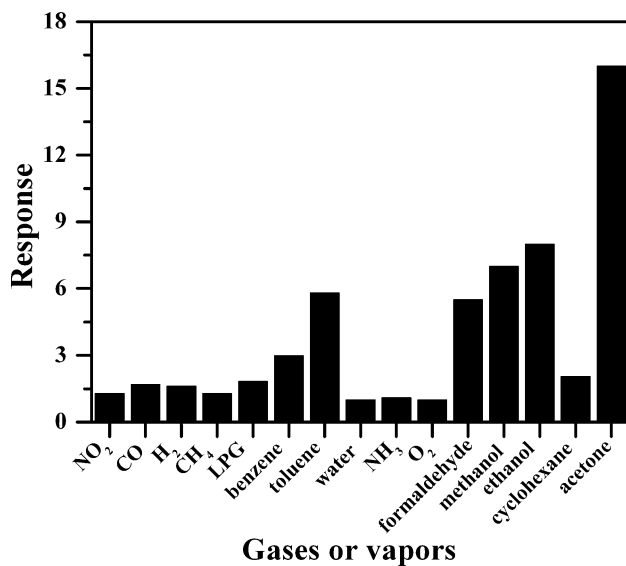
Fig. 7 Response of sample 2 sensor to various gases or vapors at 190 °C

much lower. The response of samples 1, 3, and 4 to ethanol is 4.8, 10, and 3.1, respectively, but their response to acetone was all below 5. So compared with other samples, the selectivity of sample 2 to acetone was improved. The above results revealed that the sensor based on ZnO–Fe$_2$O$_3$–ZnFe$_2$O$_4$ composite showed high anti-interference ability and could detect acetone selectively even in the presence of many kinds of interfering gases or vapors especially ethanol, which is very important for its real-time application. The long-term stability is another important factor for gas sensors. The sensor has been detected by repeating the test for many times within 60 days. No obvious variations were detected. Thus, the obtained results showed that the gas response and electrical conductance have good reproducibility.

Based on the above results, the gas-sensing mechanism of sample 2 was put forward. It is well known that the sensing mechanism of semiconductive oxide gas sensors is based on the surface reaction of semiconductive oxides [30]. The change in gas response is mainly induced by the adsorption and desorption of gas molecules from the surface of the sensing materials. When the sensing elements were exposed in air, oxygen molecules are generally chemisorbed onto the surface of the oxides as O_2^-, O^-, and O^{2-}, which exist in an equilibrium state: $O_2 \leftrightarrow O_2^- \leftrightarrow O^- \leftrightarrow O^{2-}$ [31]. According to the equilibrium, some electrons in ZnO–Fe$_2$O$_3$–ZnFe$_2$O$_4$ composite are captured and hence the decrease of the carrier concentration causes the sensing film to show a higher resistance. When the film is exposed to reductive acetone vapor at higher temperature, the surface oxygen species react with it, decreasing the surface concentration of oxygen ions, and hence increasing the carrier concentration which makes the resistance of the films reduce. The above

equilibrium, however, is exothermic. Once the operating temperature preponderates over the optimum, the concentration of oxygen ions will reduce, and then the response will decrease. So the response of ZnO–Fe$_2$O$_3$–ZnFe$_2$O$_4$ composite sensor increased upon the increase of temperature and reached the maximum at 240 °C, and then reduced at higher temperature.

The high acetone response of ZnO–Fe$_2$O$_3$–ZnFe$_2$O$_4$ composite gas sensor may be attributed to the selective promotion of acetone adsorption/oxidation by the heterostructure among ZnO, Fe$_2$O$_3$, and ZnFe$_2$O$_4$. Fe$_2$O$_3$ and ZnFe$_2$O$_4$ as dopants could enhance gas-sensing properties by changing energy-band structure, mending the morphology and surface-to-volume ratio, and creating more active sites at the grain boundaries [11]. The film of ZnO–Fe$_2$O$_3$–ZnFe$_2$O$_4$ composite with microballoons, submicron rods, and submicron particles deposited on an Al$_2$O$_3$ tube has a loosely packed structure, which provides larger channels or pores, and a higher surface area than the film of spherical or granular submicron particles. As indicated above, the specific surface area of the ZnO–Fe$_2$O$_3$–ZnFe$_2$O$_4$ composite composed of microballoons, micron rods, and micron particles was higher than that of pure ZnO and ZnO–ZnFe$_2$O$_4$ composite. Obviously, the film with a higher specific surface area can adsorb more molecules, and thus possesses a higher concentration of oxygen ions. When such film is exposed to the target gases or vapors, more adsorbed oxygen is desorbed, which leads to a bigger variation in resistance and higher response, thus improved its response/recovery characteristics. As a result, ZnO–Fe$_2$O$_3$–ZnFe$_2$O$_4$ composite gas sensor showed excellent sensing properties to acetone.

Conclusion

In summary, ZnO microbullets have been successfully synthesized in methanol or ethanol solvent, ZnO–ZnFe$_2$O$_4$ composite microbullets and ZnO–Fe$_2$O$_3$–ZnFe$_2$O$_4$ composite with microballoons, rods, and particles were synthesized in ethanol and methanol solvents, respectively. The gas-sensing measurements showed that compared with pure ZnO and ZnO–ZnFe$_2$O$_4$ composite, the ZnO–Fe$_2$O$_3$–ZnFe$_2$O$_4$ composite exhibited quicker and higher response, better selectivity, and excellent stability to acetone at relatively low temperature of 190 °C. This sensor showed strong anti-interference ability even in the presence of ethanol and was capable of detecting acetone in the range of 1–1000 ppm with excellent response/recovery characteristics. The results suggest that the synthesis method in this study has a strong influence on the morphology, composition, and gas sensing properties, indicating that solvent thermal synthesis is a simple but effective approach

for the preparation of sensing materials with high performance.

References

1. Navale SC, Ravi V, Mulla IS, Gosavi SW, Kulkarni SK (2007) Sens Actuator B 12:382
2. Zhu BL, Xie CS, Wang AH, Wu J, Wu R, Liu J (2007) J Mater Sci 42:5416. doi:10.1007/s10853-006-0768-2
3. Nenov T, Yordanov S (1992) Sens Actuator B 8:117
4. Zhang WD, Zhang WH, Ma XY (2009) J Mater Sci 44:4677. doi:10.1007/s10853-009-3716-0
5. Tien LC, Sadik PW, Norton DP, Voss LF, Pearton SJ (2005) Appl Phys Lett 87:222106
6. Shinde VR, Gujar TP, Lokhande CD (2007) Sens Actuator B 123:701
7. Chang SJ, Hsueh TJ, Chen IC, Hsieh SF, Chang SP, Hsu CL, Lin YR, Huang BR (2008) IEEE T Nano Tech 7:754
8. Kim KW, Cho PS, Kim SJ, Lee JH, Kang CY, Kim JS, Yoon SJ (2007) Sens Actuator B 123:318
9. Zhu BL, Xie CS, Wang WY, Huang KJ, Hu JH (2004) Mater Lett 58:624
10. Aygün S, Cann D (2005) Sens Actuator B 106:837
11. Ge CQ, Xie CS, Cai SZ (2007) Mater Sci Eng B 137:53
12. Tang HX, Yan M, Zhang H, Li SZ, Ma XF, Wang M, Yang DR (2006) Sens Actuator B 114:910
13. Arshak K, Gaidan I (2005) Sens Actuator B 111–112:58
14. Kuo GH, Wang HP, Hsu HH, Wang J, Chiu YM, Jou C, Hsu TF, Chen FL (2009) J Nanomater 2009: 316035 (1-3)
15. Xu JQ, Han JJ, Zhang Y, Sun YA, Xie B (2008) Sens Actuator B 132:334
16. Shishiyanu ST, Shishiyanu TS, Lupan OI (2005) Sens Actuator B 107:379
17. Gong H, Hu JQ, Wang JH, Ong CH, Zhu FR (2006) Sens Actuator B 115:247
18. Li QH, Liang YX, Wan Q, Wang TH (2004) Appl Phys Lett 85:6389
19. Lupan O, Chai GY, Chow L (2007) Microelectr J 38:1211
20. Gong H, Wang YJ, Teo SC, Huang L (1999) Sens Actuators B 54:232
21. Jing Z, Wu S (2006) Mater Lett 60:952
22. Jie Z, Hua HL, Shan G, Hui Z, Gui ZJ (2006) Sens Actuators B 115:460
23. Xie H, Yang Q, Sun X, Huang Y (2006) Sens Actuators B 113:887
24. Li X, Zhang G, Cheng F, Guo B, Chen J (2006) J Electrochem Soc 153:H133
25. Jing Z, Wang Y, Wu S (2006) Sens Actuators B 113:177
26. You LM, Huo LH, Cheng XL, Zhao H, Gao S (2008) Chin J Inorg Chem 24:1035
27. Jiang Y, Song W, Xie C, Wang A, Zeng D, Hu M (2006) Mater Lett 60:1374
28. Zhang WH, Zhang WD (2008) Sens Actuator B 134:403
29. Huang Y, Lin J, Ding XX, Tang C, Gu CZ, Qi SR (2007) Mater Lett 61:697
30. Watson J (1984) Sens Actuators 5:29
31. Huang XJ, Meng FL, Pi ZX, Xu WH, Liu JH (2004) Sens Actuators B 99:444